

Universal dynamics in the onset of a Hagen–Poiseuille flow

By Niels Asger Mortensen and Henrik Bruus

MIC – Department of Micro and Nanotechnology, NanoDTU, Technical University of Denmark, Bldg. 345 east, DK-2800 Kongens Lyngby, Denmark

(Received November 7, 2005)

The dynamics in the onset of a Hagen–Poiseuille flow of an incompressible liquid in a channel of circular cross section is well-studied theoretically. We use an eigenfunction expansion in a Hilbert space formalism to generalize the results to channels of arbitrary cross section. We find that the steady state is reached after a characteristic time scale $\tau = (\mathcal{A}/\mathcal{P})^2(1/\nu)$ where \mathcal{A} and \mathcal{P} are the cross-sectional area and perimeter, respectively, and ν is the kinematic viscosity of the liquid. For the initial dynamics of the flow rate Q for $t \ll \tau$ we find a universal linear dependence, $Q(t) = Q_\infty (\alpha/\mathcal{C}) (t/\tau)$, where Q_∞ is the asymptotic steady-state flow rate, α is the geometrical correction factor, and $\mathcal{C} = \mathcal{P}^2/\mathcal{A}$ is the compactness parameter. For the long-time dynamics $Q(t)$ approaches Q_∞ exponentially on the timescale τ , but with a weakly geometry-dependent prefactor of order unity, determined by the lowest eigenvalue of the Helmholtz equation.

1. Introduction

Hagen–Poiseuille flow (or simply Poiseuille flow) is important to a variety of applications ranging from macroscopic pipes in chemical plants to the flow of blood in veins. However, the rapid development in the field of lab-on-a-chip systems during the past decade has put even more emphasis on pressure driven laminar flow. Traditionally, capillary tubes would have circular cross-sections, but today microfabricated channels come with a variety of shapes depending on the fabrication technique in use. The list of examples includes rectangular channels obtained by hot embossing in polymer wafers, semi-circular channels in isotropically etched surfaces, triangular channels in KOH-etched silicon crystals, Gaussian-shaped channels in laser-ablated polymer films, and elliptic channels in stretched PDMS devices, see e.g. Geschke *et al.* (2004).

This development has naturally led to more emphasis on theoretical studies of shape-dependence in microfluidic channels. Recently, we therefore revisited the problem of Poiseuille flow and its shape dependence and we have also addressed mass diffusion in microchannels, Mortensen *et al.* (2005*a,b*). In the present work we combine the two former studies and address the dynamics caused by the abrupt onset of a pressure gradient at time $t = 0$ in an incompressible liquid of viscosity η and density ρ situated in a long, straight, and rigid channel of length L and some constant cross-sectional shape Ω . The solution is well-known for the case of a cylindrical channel, see e.g. Batchelor (1967), but in this paper we generalize the results to a cross-section of arbitrary shape. The similarity between mass and momentum diffusion, and the existence of a characteristic diffusion time-scale $\tau_{\text{diff}} = (\pi/4)(\mathcal{A}/\mathcal{P})^2/D$ for mass diffusion, Mortensen *et al.* (2005*b*), have led

us to introduce the momentum diffusion time-scale τ defined by

$$\tau = \left(\frac{\mathcal{A}}{\mathcal{P}}\right)^2 \frac{1}{\nu}, \quad (1.1)$$

where $\nu = \eta/\rho$ is the kinematic viscosity (having dimensions of a diffusion constant), while \mathcal{A} and \mathcal{P} is the area and perimeter of the cross section Ω , respectively. In this paper we show that the dynamics of the flow rate $Q(t)$ is universal with τ as the characteristic time scale.

As shown in Mortensen *et al.* (2005a) the shape parameters \mathcal{A} and \mathcal{P} also play an important role in the steady-state Poiseuille flow. The hydraulic resistance R_{hyd} can be expressed as

$$R_{\text{hyd}} = \alpha \frac{\eta L}{\mathcal{A}^2} \equiv \alpha R_{\text{hyd}}^*, \quad (1.2)$$

where α is a dimensionless geometrical correction factor and $R_{\text{hyd}}^* = \eta L / \mathcal{A}^2$ is a characteristic resistance. Remarkably, α is simply (linearly) related to the dimensionless compactness parameter $\mathcal{C} = \mathcal{P}^2 / \mathcal{A}$.

Above we have emphasized microfluidic flows because of the variety of shapes frequently encountered in lab-on-a-chip systems. However, our results are generally valid for laminar flows at any length scale.

2. Diffusion of momentum

We consider a long, straight channel of length L , aligned with the z -axis, having a constant cross section Ω with the boundary $\partial\Omega$ in the xy plane. The fluid flow is driven by a pressure gradient of $\nabla p = -(\Delta p/L)\mathbf{e}_x$ which is turned on abruptly at time $t = 0$. We note that strictly speaking the pressure gradient is not established instantaneously, but rather on a time-scale set by L/c where c is the speed of sound. For typical liquids $c \sim 10^3$ m/s which for micro-fluidic systems and practical purposes makes the pressure gradient appear almost instantaneously. From the symmetry of the problem it follows that the velocity field is of the form $\mathbf{v}(\mathbf{r}, t) = v(\mathbf{r}_\perp, t)\mathbf{e}_x$ where $\mathbf{r}_\perp = y\mathbf{e}_y + z\mathbf{e}_z$. From the Navier-Stokes equation it then follows that $v(\mathbf{r}_\perp, t)$ is governed by, see e.g. Batchelor (1967) or Landau & Lifshitz (1987),

$$\frac{1}{\nu} \partial_t v(\mathbf{r}_\perp, t) - \nabla^2 v(\mathbf{r}_\perp, t) = \frac{\Delta p}{\eta L}, \quad (2.1)$$

which is a diffusion equation for the momentum with the pressure drop acting as a source term on the right-hand side. The velocity v is subject to a no-slip boundary condition on $\partial\Omega$ and obviously v is initially zero, while it asymptotically approaches the steady-state velocity field $v_\infty(\mathbf{r}_\perp)$ for $t \rightarrow \infty$.

In the analysis it is natural to write the velocity as a difference

$$v(\mathbf{r}_\perp, t) = v_\infty(\mathbf{r}_\perp) - v_h(\mathbf{r}_\perp, t) \quad (2.2)$$

of the asymptotic, static field v_∞ , solving the Poiseuille problem

$$-\nabla^2 v_\infty(\mathbf{r}_\perp) = \frac{\Delta p}{\eta L}, \quad (2.3)$$

and a time-dependent field $v_h(\mathbf{r}_\perp, t)$ satisfying the homogeneous diffusion equation,

$$\frac{1}{\nu} \partial_t v_h(\mathbf{r}_\perp, t) - \nabla^2 v_h(\mathbf{r}_\perp, t) = 0. \quad (2.4)$$

From Mortensen *et al.* (2005*b*) it is known that rescaling the Helmholtz equation by $(\mathcal{A}/\mathcal{P})^2$ leads to a lowest eigenvalue a_1 that is of order unity and only weakly geometry dependent. We therefore perform this rescaling, which naturally implies the time-scale τ of Eq. (1.1) and the following form of the diffusion equation,

$$\tau \partial_t v_h(\mathbf{r}_\perp, t) - \hat{\mathcal{L}} v_h(\mathbf{r}_\perp, t) = 0. \quad (2.5)$$

where we have introduced the rescaled Laplacian $\hat{\mathcal{L}}$,

$$\hat{\mathcal{L}} \equiv \left(\frac{\mathcal{A}}{\mathcal{P}}\right)^2 \nabla^2. \quad (2.6)$$

We note that by the rescaling the Navier–Stokes equation (2.1) becomes

$$\tau \partial_t v - \hat{\mathcal{L}} v = \left(\frac{\mathcal{A}}{\mathcal{P}}\right)^2 \frac{\Delta p}{\eta L} = \frac{\alpha Q_\infty}{\mathcal{P}^2}, \quad (2.7)$$

where we have introduced the steady-state flow rate $Q_\infty = \Delta p / R_{\text{hyd}}$ and used Eq. (1.2).

3. Hilbert space formulation

In order to solve Eq. (2.7) we will take advantage of the Hilbert space formulation, Morse & Feshbach (1953), often employed in quantum mechanics, Merzbacher (1970). The Hilbert space of real functions $f(\mathbf{r}_\perp)$ is defined by the inner product

$$\langle f | g \rangle \equiv \int_{\Omega} d\mathbf{r}_\perp f(\mathbf{r}_\perp) g(\mathbf{r}_\perp) \quad (3.1)$$

and a complete set $\{|\phi_n\rangle\}$ of orthonormal basis functions,

$$\langle \phi_m | \phi_n \rangle = \delta_{nm}. \quad (3.2)$$

Above, we have used the Dirac *bra-ket* notation and δ_{nm} is the Kronecker delta. We choose the eigenfunctions $\{|\phi_n\rangle\}$ of the rescaled Helmholtz equation (with a zero Dirichlet boundary condition on $\partial\Omega$) as our basis functions,

$$-\hat{\mathcal{L}}|\phi_n\rangle = a_n|\phi_n\rangle. \quad (3.3)$$

With this complete basis any function in the Hilbert space can be written as a linear combination of basis functions. Using the *bra-ket* notation Eq. (2.7) becomes

$$\tau \partial_t |v\rangle - \hat{\mathcal{L}} |v\rangle = \frac{\alpha Q_\infty}{\mathcal{P}^2} |1\rangle. \quad (3.4)$$

The full solution Eq. (2.2) is written as

$$|v\rangle = |v_\infty\rangle - |v_h\rangle, \quad (3.5)$$

where $|v_\infty\rangle$ satisfies the Poiseuille problem Eq. (2.3),

$$-\hat{\mathcal{L}}|v_\infty\rangle = \frac{\alpha Q_\infty}{\mathcal{P}^2} |1\rangle, \quad (3.6)$$

and the homogeneous solution $|v_h\rangle$ solves the diffusion problem Eq. (2.5)

$$(\tau \partial_t - \hat{\mathcal{L}})|v_h\rangle = 0. \quad (3.7)$$

In the complete basis $\{|\phi_n\rangle\}$ we have

$$|v_h\rangle = \sum_{n=1}^{\infty} b_n e^{-a_n t/\tau} |\phi_n\rangle, \quad (3.8)$$

$$|v_\infty\rangle = \sum_{n=1}^{\infty} c_n |\phi_n\rangle, \quad (3.9)$$

and since $\lim_{t \rightarrow 0} |v_h\rangle = |v_\infty\rangle$ we have $b_n = c_n$. Multiplying Eq. (3.9) by $\langle\phi_m|$ yields

$$b_m = c_m = \langle\phi_m|v_\infty\rangle = \langle\phi_m|\hat{\mathcal{L}}^{-1}\hat{\mathcal{L}}|v_\infty\rangle = \frac{\alpha Q_\infty}{\mathcal{P}^2} a_m^{-1} \langle\phi_m|1\rangle. \quad (3.10)$$

In the second-last equality we have introduced the unit operator $1 = \hat{\mathcal{L}}^{-1}\hat{\mathcal{L}}$ and in the last equality we used the Hermitian property of the inverse Laplacian operator to let $\hat{\mathcal{L}}^{-1}$ act to the left, $\langle\phi_m|\hat{\mathcal{L}}^{-1} = -\langle\phi_m|a_m^{-1}$ from Eq. (3.3), while $\hat{\mathcal{L}}$ acts to the right, see Eq. (3.6). Substituting Eqs. (3.8) and (3.10) into Eq. (3.5) we finally obtain

$$|v\rangle = |v_\infty\rangle - \frac{\alpha Q_\infty}{\mathcal{P}^2} \sum_{n=1}^{\infty} |\phi_n\rangle \langle\phi_n|1\rangle a_n^{-1} e^{-a_n t/\tau}. \quad (3.11)$$

4. Flow rate

Using the *bra-ket* notation, the flow rate $Q(t)$ at any time is conveniently written as $Q = \langle 1|v\rangle$, and thus in steady state $Q_\infty = \langle 1|v_\infty\rangle$. Multiplying Eq. (3.11) from the left by $\langle 1|$ yields

$$Q(t) = \langle 1|v\rangle = Q_\infty - \frac{\alpha Q_\infty}{\mathcal{P}^2} \sum_{n=1}^{\infty} \langle 1|\phi_n\rangle \langle\phi_n|1\rangle a_n^{-1} e^{-a_n t/\tau}. \quad (4.1)$$

The factor $\langle 1|\phi_n\rangle \langle\phi_n|1\rangle$ is recognized as the effective area \mathcal{A}_n covered by the n th eigenfunction $|\phi_n\rangle$,

$$\mathcal{A}_n \equiv \frac{|\langle 1|\phi_n\rangle|^2}{\langle\phi_n|\phi_n\rangle} = |\langle 1|\phi_n\rangle|^2 = \langle 1|\phi_n\rangle \langle\phi_n|1\rangle. \quad (4.2)$$

The effective areas fulfil the sum-rule $\sum_{n=1}^{\infty} \mathcal{A}_n = \mathcal{A}$, seen by completeness of the basis $\{|\phi_n\rangle\}$ as follows:

$$\sum_{n=1}^{\infty} \mathcal{A}_n = \sum_{n=1}^{\infty} \langle 1|\phi_n\rangle \langle\phi_n|1\rangle = \langle 1|\left(\sum_{n=1}^{\infty} |\phi_n\rangle \langle\phi_n|\right)|1\rangle = \langle 1|1\rangle = \mathcal{A}. \quad (4.3)$$

Using the effective areas the expression Eq. (4.1) for $Q(t)$ become

$$Q(t) = \langle 1|v\rangle = Q_\infty - \frac{\alpha Q_\infty}{\mathcal{P}^2} \sum_{n=1}^{\infty} \frac{\mathcal{A}_n}{a_n} e^{-a_n t/\tau}. \quad (4.4)$$

We can find the geometrical correction factor α from Eq. (4.4) by using that $Q(0) = 0$,

$$\alpha = \mathcal{P}^2 \left(\sum_{n=1}^{\infty} \frac{\mathcal{A}_n}{a_n} \right)^{-1}, \quad (4.5)$$

and substituting into Eq. (4.4) we finally get

$$\frac{Q(t)}{Q_\infty} = 1 - \left(\sum_{n=1}^{\infty} \frac{\mathcal{A}_n}{a_n} \right)^{-1} \sum_{n=1}^{\infty} \frac{\mathcal{A}_n}{a_n} e^{-a_n t / \tau}. \quad (4.6)$$

5. Short-time dynamics

The short-time dynamics is found by Taylor-expanding Eq. (4.6) to first order,

$$\frac{Q(t)}{Q_\infty} \approx \left(\sum_{n=1}^{\infty} \frac{\mathcal{A}_n}{a_n} \right)^{-1} \mathcal{A} \frac{t}{\tau} = \frac{\alpha \mathcal{A}}{\mathcal{P}^2} \frac{t}{\tau} = \frac{\alpha}{\mathcal{C}} \frac{t}{\tau}, \quad t \ll \tau, \quad (5.1)$$

where we have used the sum-rule Eq. (4.3) for \mathcal{A}_n as well as Eq. (4.5). The short time dynamics can also be inferred directly by integration of the Navier–Stokes equation Eq. (3.4), since at time $t = 0$ we have $|v\rangle = 0$ and consequently the vanishing of velocity gradients and viscous friction, $\hat{\mathcal{L}}|v\rangle = 0$. Thus we arrive at

$$\tau \partial_t |v\rangle = \frac{\alpha Q_\infty}{\mathcal{P}^2} |1\rangle, \quad t \rightarrow 0, \quad (5.2)$$

corresponding to a constant initial acceleration throughout the fluid. Integration with respect to t is straightforward and multiplying the resulting $|v\rangle$ by $\langle 1|$ yields $Q(t)$,

$$\frac{Q(t)}{Q_\infty} \simeq \frac{\alpha}{\mathcal{P}^2} \langle 1|1\rangle \frac{t}{\tau} = \frac{\alpha \mathcal{A}}{\mathcal{P}^2} \frac{t}{\tau} = \frac{\alpha}{\mathcal{C}} \frac{t}{\tau}, \quad t \ll \tau. \quad (5.3)$$

Thus initially, the fluid responds to the pressure gradient in the same way as a rigid body responds to a constant force.

6. Long-time dynamics

As the flow rate increases, friction sets in, and in the long-time limit $t \gg \tau$ the flow-rate saturates at the value Q_∞ where there is a balance between the pressure gradient and frictional forces. For the long-time saturation dynamics the lowest eigenstate plays the dominating role and taking only the $n = 1$ term in Eq. (4.6) we obtain

$$\frac{Q(t)}{Q_\infty} \simeq 1 - e^{-a_1 t / \tau}, \quad t \gg \tau / a_2, \quad (6.1)$$

where we have used that the lowest eigenvalue a_1 is non-degenerate to truncate the summation.

The time it takes to reach steady-state is denoted τ_∞ . A lower bound τ_1 for τ_∞ can be obtained from Eq. (5.3) by assuming that the initial acceleration is maintained until $Q(\tau_1)/Q_\infty = 1$ is reached,

$$\tau_\infty > \tau_1 = \frac{\mathcal{C}}{\alpha} \tau. \quad (6.2)$$

A better estimate τ_2 for τ_∞ is obtained from Eq. (6.1) by demanding $Q(\tau_2)/Q_\infty = 1 - e^{-3}$.

$$\tau_\infty \approx \tau_2 = \frac{3}{a_1} \tau. \quad (6.3)$$

Using the parameter values for the circle listed in Table 1 we find the values

$$\tau_1 = 0.5 \tau < \tau_2 = 2.1 \tau \approx \tau_\infty. \quad (6.4)$$

7. Numerical results

Only few geometries allow analytical solutions of both the Helmholtz equation and the Poisson equation. The circle is of course the most well-known example, but the equilateral triangle is another exception. However, in general the equations have to be solved numerically, and for this purpose we have used the commercially available finite-element software Comsol 3.2 (see www.comsol.com). Numbers for a selection of geometries are tabulated in Table 1.

The circle is the most compact shape and consequently it has the largest value for $\mathcal{A}_1/\mathcal{A}$, i.e., the mode has the relatively largest spatial occupation of the total area. The eigenvalue a_1 is of the order unity for compact shapes and in general it tends to increase slightly with increasing values of \mathcal{C} . The modest variation from geometry to geometry in both a_1 and the other parameters suggests that the dynamics of $Q(t)$ will appear almost universal.

In order to illustrate the validity of our two asymptotic expressions, Eqs. (5.3) and (6.1), we have compared them using the values for a circular shape to time-dependent finite-element simulations of Eq. (2.1). As illustrated in Fig. 1 we find a perfect agreement between the asymptotic expressions Eqs. (5.3) and (6.1) and the numerically exact data for a circle, a square, and an equilateral triangle. Comparing the corresponding parameters in Table 1 we would expect all data to almost coincide, which is indeed also observed in Fig. 1. The small spread in eigenvalues and other parameters thus gives rise to close-to-universal dynamics. From the plot it is also clear that τ is indeed a good estimate for the time it takes to reach the steady state.

8. Conclusions

In conclusion, by using a compact Hilbert space formalism we have shown how the initial dynamics in the onset of Poiseuille flow is governed by a universal linear raise in flow rate $Q(t)$ over a universal time-scale τ above which it saturates exponentially to the steady-state value Q_∞ . The steady state is reached after a time $\tau_\infty \approx \mathcal{C}\tau/\alpha$. Apart from being a fascinating example of universal dynamics for a complex problem our results may have important applications in design of real-time programmable pressure-driven micro-fluidic networks.

We would like to acknowledge stimulating discussions with F. Okkels.

REFERENCES

- BATCHELOR, G. K. 1967 *An Introduction to Fluid Dynamics*. Cambridge: Cambridge University Press.
- BRACK, M. & BHADURI, R. K. 1997 *Semiclassical Physics*. New York: Addison Wesley.
- GESCHKE, O., KLANK, H. & TELLEMAN, P., ed. 2004 *Microsystem Engineering of Lab-on-a-Chip Devices*. Weinheim: Wiley-VCH Verlag.
- LANDAU, L. D. & LIFSHITZ, E. M. 1987 *Fluid Mechanics*, 2nd edn., *Landau and Lifshitz, Course of Theoretical Physics*, vol. 6. Oxford: Butterworth-Heinemann.
- MERZBACHER, E. 1970 *Quantum Mechanics*. New York: Wiley & Sons.
- MORSE, P. M. & FESHBACH, H. 1953 *Methods of Theoretical Physics*. New York: McGraw-Hill.
- MORTENSEN, N. A., OKKELS, F. & BRUUS, H. 2005a Reexamination of Hagen-Poiseuille flow: Shape dependence of the hydraulic resistance in microchannels. *Phys. Rev. E* **71**, 057301.
- MORTENSEN, N. A., OKKELS, F. & BRUUS, H. 2005b Universality in edge-source diffusion dynamics. *preprint* <http://arxiv.org/cond-mat/0510627>.

shape	a_1	$\mathcal{A}_1/\mathcal{A}$	α/C
circle	$\gamma_{0,1}^2/4 \simeq 1.45^a$	$4/\gamma_{0,1}^2 \simeq 0.69^a$	2^b
quarter-circle	1.27^c	0.65^c	1.85^c
half-circle	1.38^c	0.64^c	1.97^c
ellipse(1:2)	1.50^c	0.67^c	2.10^c
ellipse(1:3)	1.54^c	0.62^c	2.21^c
ellipse(1:4)	1.57^c	0.58^c	2.28^c
triangle(1:1:1)	$\pi^2/9 \simeq 1.10^d$	$6/\pi^2 \simeq 0.61^d$	$5/3 \simeq 1.67^b$
triangle(1:1: $\sqrt{2}$)	$\frac{5\pi^2}{4(2+\sqrt{2})^2} \simeq 1.06^a$	$512/9\pi^4 \simeq 0.58^a$	1.64^c
square	$\pi^2/8 \simeq 1.23^a$	$64/\pi^4 \simeq 0.66^a$	1.78^c
rectangle(1:2)	$5\pi^2/36 \simeq 1.37^a$	$64/\pi^4 \simeq 0.66^a$	1.94^c
rectangle(1:3)	$5\pi^2/32 \simeq 1.54^a$	$64/\pi^4 \simeq 0.66^a$	2.14^c
rectangle(1:4)	$17\pi^2/100 \simeq 1.68^a$	$64/\pi^4 \simeq 0.66^a$	2.28^c
rectangle(1: ∞)	$\sim \pi^2/4 \simeq 2.47^a$	$64/\pi^4 \simeq 0.66^a$	$\sim 3^e$
pentagon	1.30^c	0.67^c	1.84^c
hexagon	1.34^c	0.68^c	1.88^c

TABLE 1. Central parameters for the lowest eigenfunction for different cross sectional shapes. Note how the different numbers converge when going through the regular polygons starting from the triangle(1:1:1) through the square, the pentagon, and the hexagon to the circle.

^aSee e.g. Morse & Feshbach (1953) for the eigenmodes and eigenspectrum.

Here $\gamma_{0,1}$ denotes the first root of the zeroth Bessel function of the first kind.

^bSee Mortensen *et al.* (2005a).

^cData obtained by finite-element simulations.

^dSee e.g. Brack & Bhaduri (1997) for the eigenmodes and eigenspectrum.

^eSee e.g. Batchelor (1967) for a solution of the Poisson equation.

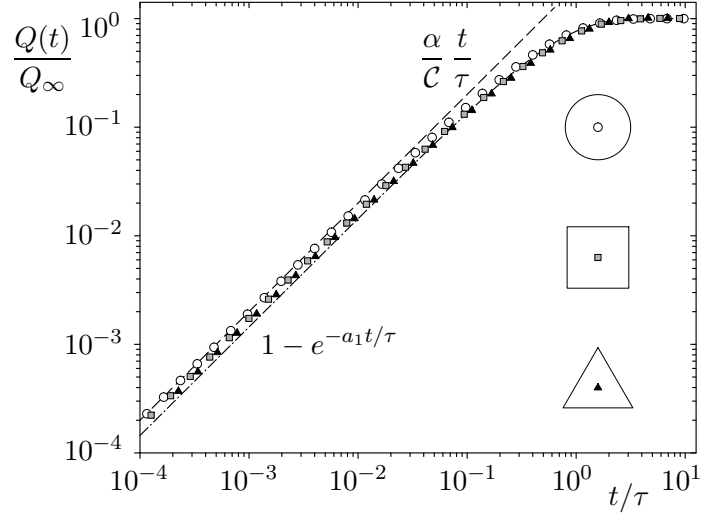


FIGURE 1. A log-log plot of the flow rate $Q(t)/Q_\infty$ as a function of time t/τ . The dashed line is the short-time approximation Eq. (5.3), while the dashed-dotted line is the long-time approximation Eq. (6.1), both for the case of a circle, i.e., using $C/\alpha = 2$ and $a_1 = 1.45$ as listed in Table 1. The data points are the results of time-dependent finite-element simulations for the cases of the cross section being a circle (white circles), a square (gray squares), and an equilateral triangle (black triangles).